

Electron mean-free path in metal-coated nanowires

Alexander Moroz

Wave-scattering.com

(wave-scattering@yahoo.com)

Received January 4, 2011; accepted March 1, 2011;
posted March 15, 2011 (Doc. ID 140424); published April 18, 2011

The mean-free path L_{eff} is calculated for a circular shell geometry under the assumptions of (i) billiard scattering and (ii) diffusive scattering. Similarly to a spherical shell geometry, L_{eff} displays qualitatively different behavior on the shell thickness D for the two models. Whereas, for the billiard model $L_{\text{eff}} = \pi D/2$, the mean-free path in the diffusive scattering case is a complicated function involving complete and incomplete elliptic integrals of the first, second, and third kinds. Nevertheless, a linear combination of D and $D \ln(R/2D)$, where R is the outer circle radius, is shown to capture the functional dependence of L_{eff} in the diffusive scattering case remarkably well over almost the entire parameter range. Hopefully, future experiments on single and well-controlled dielectric-core-metal-shell nanowires could differentiate between the two models. © 2011 Optical Society of America

OCIS codes: 350.4238, 350.4990, 240.6680.

1. INTRODUCTION

Metal nanoparticles (MNPs) have been playing an increasingly important role in modifying fluorescence rates for addressing various issues of interest to biology [1–5], solar energy conversion [6], localized surface plasmon resonance (LSPR) sensing [7–13], and surface-enhanced spectroscopies [14,15]. The performance of individual MNPs in the above applications is crucially influenced by the LSPR homogeneous line width—the full width at half-maximum (fwhm) Γ —or, alternatively, the LSPR dephasing time $T_2 = 2\hbar/\Gamma$ [16,17]. The standard classical approach for describing the size dependence of the dielectric function assumes that, if a particle size is comparable to or smaller than the mean-free path of free conduction electrons in the bulk material, ℓ_∞ (42 nm for gold [18], 52 nm for silver [19,20], and 45 nm for Cu [20]), the scattering of conduction electrons from the particle surface results in a reduced effective mean-free path, $L_{\text{eff}} < \ell_\infty$, called the *free-path effect* [18,19,21–23]. For particles small enough that retardation effects are not significant (i.e., with k being a wave vector, one can ignore k^2 - and k^3 -dependent terms in the particle polarizability [24]), and whose spectra are dominated by a single plasmon resonance, the LSPR resonance linewidth is, according to the Mathiessen's rule, given by [18,19,21–23]

$$\Gamma = \Gamma_0 + \frac{v_F}{L_{\text{eff}}}. \quad (1)$$

The first term, $\Gamma_0 = v_F/\ell_\infty$, on the right-hand side accounts for bulk effects and describes the intrinsic bulk width of the dipole plasmon polariton. The second term, comprising the Fermi velocity v_F of conduction electrons (1.38×10^6 m/s for gold and 1.39×10^6 m/s for silver [22]), accounts for the surface scattering. Indeed, the ratio v_F/L_{eff} may be interpreted classically as the effective rate of scattering of a conduction electron off the particle surface. The surface scattering induces a size-dependent correction to the dielectric function ϵ_b of a bulk metal. The contribution of free electrons to the dielectric function is described by the familiar *causal* and (during collisions) *electron number conserving* Drude-like dielectric function:

$$\epsilon_D(\omega) = 1 - \frac{\omega_p^2}{\omega(\omega + i\gamma)}, \quad (2)$$

where ω_p and γ are the plasma frequency and damping constant (which also account for elastic scattering), respectively. A standard approach to incorporate the free-path effect, or the size correction, is to replace ϵ_b by [19]

$$\epsilon_m(\omega) = \epsilon_b(\omega) - \epsilon_{D,b}(\omega) + \epsilon_{D,sd}(\omega), \quad (3)$$

where $\epsilon_{D,b}$ is the Drude dielectric function describing free conduction electrons of the bulk metal with the bulk damping constant $\gamma = \Gamma_0$, whereas the term $\epsilon_{D,sd}$ differs from $\epsilon_{D,b}$ in that Γ_0 is replaced by the size-corrected value Γ . Obviously, the above described subtraction and addition of the Drude-like terms with different damping constants has the net effect of renormalizing the damping constant of *free conduction electrons* from their bulk value Γ_0 to Γ . The size correction has to be taken into account if MNP properties, such as the quality factor Q of the resonance at an energy E_{res} ($Q = E_{\text{res}}/\Gamma$) and the local field enhancement factor $|f|$ (in a harmonic model $|f| = Q$), are to be accurately modeled [16,17]. It constitutes an intrinsic limit to the LSPR width in small particles and is thus a limiting factor in the possible size reduction for many applications.

Classically, the mean-free path L_{eff} is calculated as the *average chord length between one point on the surface and any other point, averaged, with a suitable probability measure, over all points on the surface as the initial point*. According to the Euler *diffusive* surface scattering model [21], the electron reflection on the boundary surface is taken to be fully *isotropic*, meaning there is equal probability for an electron to be scattered at any angle with respect to the surface normal \mathbf{n} . For that reason, the model is sometime referred to as the isotropic scattering model [22]. In the *billiard* case, one weights the chords with the cosine of the angle between the chord and the surface normal [25–27]. Provided that the cosine reflects the physical probability of the chords upon the surface scattering, the radiant intensity from an electron

enclosure surface would be proportional to the cosine of the angle θ between the observer's line of sight and the surface normal \mathbf{n} . Thereby, an area element on the surface when viewed from any angle would have the same radiance, turning the electron enclosure surface into a “Lambertian” surface [27]. The difference in the surface scattering description is then reflected in different probability measures [see Eqs. (7) and (8)].

Following our earlier treatment of a mean-free path in a spherical shell geometry [27], the focus of this article is on elongated wire-, or cylindrical-, like structures. As first suggested in [28], elongated metal nanowires can be prepared by filling the pores of deep etched silicon substrates and thereby obtaining two-dimensional (2D) photonic crystals with a complete photonic bandgap in the visible [28]. Alternatively, isolated metallic nanowires can be synthesized using template-directed electrosynthetic techniques [29], or a structured pattern of nanoscale metal wires can be formed in a microstructured silica fiber [30]. The emphasis here shall be on elongated *core-shell* structures. In nanophotonics and nanoplasmonics, a coaxial metal–dielectric–metal structure, a dielectric–metal–dielectric tube structure, together with a metal tube with either (i) a central hole or (ii) two parallel holes, have all been considered for guiding of a one-dimensional optical beam with nanometer diameter [31]. By using suspended single-wall carbon nanotubes as substrates for deposition of various metals by evaporation, individual metal nanowires 10 nm wide and with continuous length up to tens of micrometers can be fabricated [32]. Alternatively, a 2D array of silicon posts can be coated with metals, thereby preparing 2D plasmonic waveguiding structures with enhanced photonic bandgaps [33]. However, contrary to the case of spherical or spheroidal particles [16–19,21–23], the necessity in using a size-corrected dielectric function [Eq. (3)] for elongated structures has received little attention, even though the effect is expected to be more pronounced than the effect of the so-called *nonlocal* dielectric function (see [34]).

Provided one is only interested in the propagation in the transversal direction (e.g., electric field intensity oriented perpendicular to the cylinder axis), the core–shell problem reduces to the calculation of a mean-free path in a circular shell region that is (i) neither *convex* nor (ii) *simply connected*. This means that the early results by Cauchy [35,36], Czuber [37], Dirac [38], Weinberg and Wigner [39], and others [40–42], which yield the mean-free path in terms of the geometrical parameters of a *convex* domain Ω in d spatial dimensions, can no longer be applied. Nevertheless, in the billiard case, one could still apply a general geometric formula [25,26]:

$$L_B = \frac{|\Omega| \cdot |S^{d-1}|}{|\partial\Omega| \cdot |B^{d-1}|}. \quad (4)$$

The formula reduces to the Cauchy formula for *convex* domains but its validity is much broader—any *bounded and connected* domain [25,26]. Here $|\Omega|$ is the d -dimensional volume (i.e., the area for $d = 2$) of Ω , $|\partial\Omega|$ is the area of the $(d - 1)$ -dimensional surface $\partial\Omega$ (i.e., the total circumference for $d = 2$) of Ω , $|S^{d-1}|$ is the surface of a unit sphere in \mathbb{R}^d , and $|B^{d-1}| = |S^{d-2}|/(d - 1)$ is the volume of a unit ball in \mathbb{R}^{d-1} . One has

$$S^1 = 2\pi, \quad S^2 = 4\pi, \quad B^1 = 2, \quad B^2 = \pi. \quad (5)$$

The outline of the article is as follows. In Section 2 we summarize notation and give some basic definitions. Since only an abstract proof of the general geometric billiard formula in Eq. (4) exists [25,26], it is regarded expedient to illustrate its validity on some special cases that are outside the reach of early theories by Cauchy [35,36] and others [37–42]. This is done in Section 3, where the billiard formula in Eq. (4) is confirmed in the cylindrical shell case by an explicit averaging procedure. The mean-free path L_d for the case of the diffusive scattering is calculated in Section 4. Quite surprisingly, unlike in a spherical shell geometry [27], L_d cannot be expressed in terms of elementary functions. Nevertheless, it is possible to determine a two-term asymptotic, which can be used instead of the exact formula over almost the entire parameter range. In Section 5 various conditions of the applicability of our results are discussed (see Fig. 4). We then conclude by Section 6. A number of formulas and intermediary steps are relegated to Appendix A.

2. NOTATION AND DEFINITIONS

Let r_1 and r_2 be the radii of the inner and outer surfaces of the cylindrical shell, respectively [see Figs. 1 and 2]. Following the notation of [27] and its online supplement, let us introduce at any point P of the boundary surface $\partial\Omega$ of Ω coordinates with the origin at P , with θ being the angle between the chord and the inward normal at P . Let $L(\theta)$ be the length of the straight chord line PP' at an angle θ to the inward normal at P connecting the point P with a conjugate boundary point P' . The averaging over different chord lengths $L(\theta)$ emanating from P involves an integration over the angle of π above the tangent plane at the point P , i.e., with the integration range $\theta \in (-\pi/2, \pi/2)$:

$$\ell_P = \int L(\theta) d\mu(\theta). \quad (6)$$

Because of the symmetry of the problem, the range of integration in Eq. (6) can be reduced to $\theta \in (0, \pi/2)$ with the probability measure

$$d\mu_B(\theta) = \cos\theta d\theta, \quad (7)$$

in the *billiard* case, and

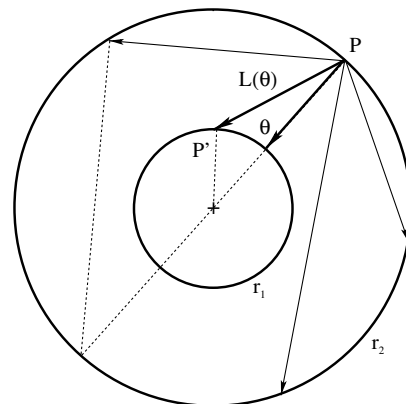


Fig. 1. Cylindrical shell geometry and the definition of parameters for a point on the outer shell boundary. The chord length $L(\theta)$ is given by Eq. (12). Typical triangles used to calculate $L(\theta)$ are shown by dashed lines.

$$d\mu_d(\theta) = \frac{2}{\pi} d\theta, \tag{8}$$

in the *diffusive scattering* case. The resulting mean free path is defined as

$$L_{\text{eff}} = \frac{\int_{\partial\Omega} \ell_P dS}{|\partial\Omega|}. \tag{9}$$

In virtue of the cylindrical symmetry, for all the points on the shell–ambient interface, the very same average chord length $\ell_P = \ell_2$ is obtained after performing the integral in Eq. (6). Similarly, all the points on the shell–core interface are equivalent when the value of the integral in Eq. (6) is concerned; in this case, we denote the average chord length by ℓ_1 . Consequently, the surface integral in Eq. (9) is replaced by a simple algebraic relation:

$$L_{\text{eff}} = \frac{r_2 \ell_2 + r_1 \ell_1}{r_2 + r_1}. \tag{10}$$

Given the radii r_1 and r_2 of the inner and outer surfaces of the cylindrical shell, respectively, it turns out expedient to additionally introduce shorthands $R = r_2$, $D = r_2 - r_1$, and $q = r_1/r_2$.

A. Point Located on the Outer Shell Boundary

As shown in Fig. 1, one distinguishes two sets of trajectories: the first set of trajectories occurs when $|\sin \theta| \leq r_1/r_2$, whereas the second set of trajectories takes place when $|\sin \theta| > r_1/r_2$. The separation point between the two different sets of trajectories is

$$|\sin \theta_c| = r_1/r_2 = q. \tag{11}$$

In accord with the integration range, θ_c will be taken as a positive number from the interval $(0, \pi/2)$. The corresponding lengths of the two sets of trajectories as a function of θ are then [27]

$$L(\theta) = \begin{cases} r_2 \cos \theta - \sqrt{r_1^2 - r_2^2 \sin^2 \theta}, & |\theta| \leq \theta_c \\ 2r_2 \cos \theta, & |\theta| > \theta_c \end{cases}. \tag{12}$$

The upper formula follows on applying the law of cosines for a triangle formed by the sides of length L , r_1 , and r_2 (see also Fig. 1), and solving a quadratic equation for L . The lower formula follows on using an elementary definition of cosine for a right-angled triangle circumscribed by a circle. Upon substituting Eq. (12) into the integral in Eq. (6), for ℓ_2 , one finds

$$\ell_2 = S_1 + S_3 - S_2, \tag{13}$$

with

$$S_1 = 2r_2 \int_{\theta_c}^{\pi/2} \cos \theta d\mu(\theta), \tag{14}$$

$$S_2 = \int_0^{\theta_c} \sqrt{r_1^2 - r_2^2 \sin^2 \theta} d\mu(\theta), \tag{15}$$

$$S_3 = r_2 \int_0^{\theta_c} \cos \theta d\mu(\theta). \tag{16}$$

Obviously [see Eq. (11)] $\theta_c \rightarrow 0$ in the limit $r_1 \rightarrow 0$. One then recovers from Eq. (10) the special case of a homogeneous circle, in which case [41]

$$L_{\text{eff}} \equiv \ell_2 = S_1(\theta_c = 0) = \begin{cases} \pi R/2, & \text{billiard scattering} \\ 4R/\pi, & \text{diffusive scattering} \end{cases}. \tag{17}$$

B. Point Located on the Inner Shell Boundary

For points on the *inner* shell boundary, or, on the shell–core interface (see Fig. 2), it turns out that the integral in Eq. (6) with the billiard and diffusive can be more easily performed in the coordinates with the origin coinciding with the centers of the two concentric circles forming the shell boundaries. In what follows, the coordinates at point P will be referred to as the θ -coordinates, and the latter coordinates as the θ' -coordinates. (See Fig. 2 for θ and θ' definitions.) Summarizing the results of [27], on applying the law of cosines, the chord length in the θ' -coordinates is

$$L(\theta') = [r_1^2 + r_2^2 - 2r_1 r_2 \cos \theta']^{1/2}. \tag{18}$$

The angle θ' is limited within the interval for which $\cos \theta' \in (1, r_1/r_2)$, i.e., $\theta' \in (0, \theta'_m)$, where [see Eq. (11)]

$$\cos \theta'_m = q = r_1/r_2. \tag{19}$$

Similarly to a spherical shell case [27], it turns out expedient to introduce a shorthand

$$\beta = \frac{r_1^2 + r_2^2}{2r_1 r_2} \geq 1, \tag{20}$$

which obeys the following straightforward relations:

$$\beta \pm 1 = \frac{(r_2 \pm r_1)^2}{2r_1 r_2}, \tag{21}$$

$$\beta - (r_1/r_2) = \frac{r_2^2 - r_1^2}{2r_1 r_2}, \tag{22}$$

$$\beta^2 - 1 = \frac{(r_2^2 - r_1^2)^2}{(2r_1 r_2)^2}. \tag{23}$$

To this end, recast $L(\theta')$ in Eq. (18) in terms of $x = \cos \theta'$ and β [27]:

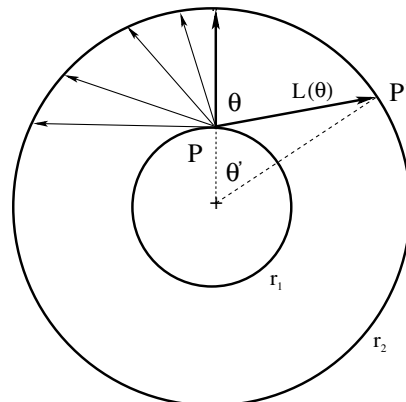


Fig. 2. Cylindrical shell geometry and the definition of parameters for a point on the inner shell boundary. The chord length L in θ' -coordinates is given by Eqs. (18) and (24). A triangle used to calculate the highlighted chord length L by the cosine formula $c^2 = a^2 + b^2 - 2ab \cos \theta$ in θ' -coordinates is shown by dashed lines.

$$L(\theta') = \sqrt{2r_1r_2(\beta - x)^{1/2}}. \tag{24}$$

For future convenience, the following two formulas are given:

$$\cos \theta d\theta = \frac{r_2}{L(\theta')} \left[x - \frac{1-x^2}{2(\beta-x)} \right] d\theta', \tag{25}$$

$$d\theta = \left[x - \frac{1-x^2}{2(\beta-x)} \right] \frac{d\theta'}{x - (r_1/r_2)}. \tag{26}$$

3. BILLIARD SCATTERING

According to the general billiard formula in Eq. (4), one gets for planar billiards ($d = 2$)

$$L_B = \frac{\pi|\Omega|}{|\partial\Omega|}. \tag{27}$$

Then, in the special case of a circular shell,

$$L_B = \frac{\pi}{2}(r_2 - r_1). \tag{28}$$

In this section, the billiard formula in Eq. (28) will be confirmed by an explicit averaging according to Eq. (10) with the respective ℓ_1 and ℓ_2 calculated with the reduced probability measure $d\mu_B$ given by Eq. (7).

A. Point Located on the Outer Shell Boundary

On performing the respective integrals in Eqs. (14)–(16) with the probability measure $d\mu_B$ [Eq. (7)] one finds

$$S_1 = 2r_2 \int_{\theta_c}^{\pi/2} \cos^2 \theta d\theta = r_2 \left(\frac{\pi}{2} - \theta_c \right) - r_1 \sqrt{1 - q^2}, \tag{29}$$

$$S_3 = r_2 \int_0^{\theta_c} \cos^2 \theta d\theta = r_2 \frac{\theta_c}{2} + \frac{r_1}{2} \sqrt{1 - q^2}. \tag{30}$$

In arriving at the above results for S_1 and S_3 , we have used Eq. (A1) and that [see Eq. (11)]

$$\sin 2\theta_c = 2 \sin \theta_c \cos \theta_c = 2q\sqrt{1 - q^2}. \tag{31}$$

Regarding

$$S_2 = \int_0^{\theta_c} \sqrt{r_1^2 - r_2^2 \sin^2 \theta} \cos \theta d\theta = r_2 \int_0^q \sqrt{q^2 - t^2} dt, \tag{32}$$

where $t = \sin \theta$, the integral can be readily performed on using Eq. (A2):

$$S_2 = r_2 \left(\frac{t}{2} \sqrt{q^2 - t^2} + \frac{q^2}{2} \arcsin \frac{t}{q} \right) \Big|_0^q = \frac{\pi r_1^2}{4r_2}. \tag{33}$$

Thus, the mean-free path in a billiard measure for a point located on the outer shell boundary is

$$\begin{aligned} \ell_2 &= S_1 + S_3 - S_2 \\ &= \frac{r_2}{2} [\pi - \arcsin(r_1/r_2)] - \frac{r_1}{2} \sqrt{1 - (r_1/r_2)^2} - \frac{\pi r_1^2}{4r_2}, \end{aligned} \tag{34}$$

where we have substituted [see Eq. (11)]

$$\theta_c = \arcsin(r_1/r_2). \tag{35}$$

Obviously,

$$\ell_2 \rightarrow \frac{\pi r_2}{2} \quad (r_1 \rightarrow 0). \tag{36}$$

The limiting value is the billiard mean-free path for a homogeneous cylinder [see Eq. (17)].

B. Point Located on the Inner Shell Boundary

Upon using consecutively Eqs. (24) and (25),

$$L(\theta) \cos \theta d\theta = r_2 \left[x - \frac{(1-x^2)}{2(\beta-x)} \right] d\theta', \tag{37}$$

where $x = \cos \theta'$. Hence

$$\ell_1 = r_2 \int_0^{\theta'_m} \left[x - \frac{(1-x^2)}{2(\beta-x)} \right] d\theta' = C_1 + C_2, \tag{38}$$

where [see Eq. (19)]

$$C_1 = r_2 \int_0^{\theta'_m} \cos \theta' d\theta' = r_2 \int_0^{\sqrt{1-q^2}} dx = r_2 \sqrt{1 - q^2}, \tag{39}$$

and (with minus sign in Eq. (38) absorbed in the denominator)

$$\begin{aligned} C_2 &= \frac{r_2}{2} \int_0^{\theta'_m} \frac{1-x^2}{x-\beta} d\theta' = \frac{r_2}{2} \int_q^1 \frac{\sqrt{1-x^2}}{x-\beta} dx \\ &= \frac{r_2}{2} \left[\sqrt{1-x^2} - \beta \arcsin x + \sqrt{\beta^2 - 1} \arcsin \frac{1-\beta x}{x-\beta} \right] \Big|_q^1 \\ &= \frac{r_2}{2} \left[\frac{\pi}{2} (\sqrt{\beta^2 - 1} - \beta) - \sqrt{1 - q^2} + (\sqrt{\beta^2 - 1} + \beta) \arcsin q \right] \\ &= -\frac{\pi r_1}{4} - \frac{r_2}{2} \sqrt{1 - q^2} + \frac{r_2^2}{2r_1} \arcsin q. \end{aligned} \tag{40}$$

The integral C_2 has been performed on using the quadrature formula in Eq. (A3). In arriving at the result for C_2 , we have used Eq. (A7) and [see Eqs. (20) and (23)] that

$$\sqrt{\beta^2 - 1} \mp \beta = \begin{cases} -q \\ 1/q \end{cases}. \tag{41}$$

Note that, within the integration range,

$$x \geq r_1/r_2, \quad x \leq 1 \leq \beta = \frac{r_1^2 + r_2^2}{2r_1r_2}. \tag{42}$$

On combining the partial results of Eqs. (39) and (40), one finds

$$\ell_1 = C_1 + C_2 = \frac{r_2}{2} \sqrt{1 - (r_1/r_2)^2} - \frac{\pi r_1}{4} + \frac{r_2^2}{2r_1} \arcsin(r_1/r_2). \tag{43}$$

In virtue of $\arcsin r_1/r_2 \sim r_1/r_2$ as $r_1 \rightarrow 0$, one has $\ell_1 \rightarrow R$ in the limit $r_1 \rightarrow 0$.

C. Final Result

On combining Eqs. (34) and (43),

$$r_2 \ell_2 + r_1 \ell_1 = \frac{\pi}{2} (r_2^2 - r_1^2). \tag{44}$$

The billiard formula in Eq. (28) for the resulting mean free path L_B is now straightforwardly recovered upon substituting the partial result in Eq. (44) into the averaging formula in Eq. (10).

4. DIFFUSIVE SCATTERING

A. Point Located on the Outer Shell Boundary

The respective integrals in Eqs. (14) and (16) with the measure $d\mu_d$ given by Eq. (8) can be straightforwardly performed:

$$S_1 = \frac{4r_2}{\pi} \int_{\theta_c}^{\pi/2} \cos \theta d\theta = \frac{4}{\pi} (r_2 - r_1), \tag{45}$$

$$S_3 = \frac{2r_2}{\pi} \int_0^{\theta_c} \cos \theta d\theta = \frac{2}{\pi} r_1. \tag{46}$$

The integral in Eq. (15) is recast as

$$S_2 = \frac{2r_1}{\pi} \int_0^{\theta_c} \sqrt{1 - (1/q)^2 \sin^2 \theta} d\theta. \tag{47}$$

The latter integral can be expressed [see Eq. (1.5.36.1) of [43]] as

$$\begin{aligned} S_2 &= \frac{2}{\pi} \left\{ r_2 E[\arcsin[(\sin \theta)/q], q^2] \right. \\ &\quad \left. - r_1 \left(\frac{r_2}{r_1} - \frac{r_1}{r_2} \right) F[\arcsin[(\sin \theta)/q], q^2] \right\}_0^{\theta_c} \\ &= \frac{2}{\pi} r_2 E(q^2) - \frac{2}{\pi} \frac{r_2^2 - r_1^2}{r_2} K(q^2), \end{aligned} \tag{48}$$

where we have made use of Eqs. (11), (A8), and (A9), and $K(q^2) \equiv F(\pi/2, q^2)$ and $E(q^2) \equiv E(\pi/2, q^2)$ denote the complete elliptic integrals of the first and second kind, respectively [see Eqs. (17.3.1-4) of [44]]. Eventually,

$$\ell_2 = S_1 + S_3 - S_2 = \frac{2}{\pi} \left[2r_2 - r_1 - r_2 E(q^2) + \frac{r_2^2 - r_1^2}{r_2} K(q^2) \right]. \tag{49}$$

For completeness, in the limit $r_1 \rightarrow 0$, one finds on using Eq. (A11)

$$\ell_2 \sim \frac{2}{\pi} \{ 2r_2 - r_1 + r_2 [F(q^2) - E(q^2)] \} \rightarrow \frac{4r_2}{\pi} \quad (r_1 \rightarrow 0). \tag{50}$$

As expected, the result in Eq. (17) for a homogeneous cylinder is recovered in the limit $r_1 \rightarrow 0$.

B. Point Located on the Inner Shell Boundary

On using consecutively Eqs. (24) and (25) with $x = \cos \theta'$,

$$L(\theta) d\theta = \sqrt{2r_1 r_2} \left[x - \frac{1-x^2}{2(\beta-x)} \right] \frac{(\beta-x)^{1/2}}{x-q} d\theta'. \tag{51}$$

Thus

$$\ell_1 = \frac{2}{\pi} \int_0^{\theta_m} L(\theta) d\theta = C_1 - C_2, \tag{52}$$

where

$$C_1 = \frac{2}{\pi} \sqrt{2r_1 r_2} \int_0^{\theta_m} \frac{x(\beta-x)^{1/2}}{x-q} d\theta', \tag{53}$$

$$\begin{aligned} C_2 &= \frac{2}{\pi} \sqrt{\frac{r_1 r_2}{2}} \int_0^{\theta_m} \frac{(1-x^2)}{(x-q)(\beta-x)^{1/2}} d\theta' \\ &= \frac{2}{\pi} \sqrt{\frac{r_1 r_2}{2}} \int_q^1 \frac{\sqrt{1-x^2}}{(x-q)(\beta-x)^{1/2}} dx. \end{aligned} \tag{54}$$

One finds

$$\begin{aligned} C_1 &= -\frac{4i}{\pi} \sqrt{\frac{2r_1 r_2}{\beta-1}} \{ (1+q-\beta) F(\arcsin \phi_1, m) \\ &\quad - q \Pi(n, \arcsin \phi_1, m) + (\beta-1) E(\arcsin \phi_1, m) \} \Big|_{x=1}^q, \end{aligned} \tag{55}$$

where Π is an incomplete elliptic integral of the third kind [see Eq. (17.2.14) of [44] with $m = \sin^2 \alpha$; see also Eq. (A10)]:

$$\begin{aligned} \phi_1 = \phi_1(x) &= \sqrt{\frac{\beta-x}{\beta+1}} < 1, & m &= \frac{\beta+1}{\beta-1} > 1, \\ n &= \frac{\beta+1}{\beta-q} > 1. \end{aligned} \tag{56}$$

Note that the inequalities in Eq. (42) hold within the integration range. On the other hand,

$$\begin{aligned} C_2 &= \frac{4}{\pi} \sqrt{\frac{r_1 r_2}{2}} \sqrt{\frac{1-q^2}{\beta-q}} + \frac{4i}{\pi} \sqrt{\frac{r_1 r_2}{2}} \left\{ \frac{(1-q^2)}{\sqrt{\beta+1}(\beta-q)} \right. \\ &\quad \times \Pi \left(\frac{\beta-q}{\beta+1}; \Phi_2 \left| \frac{\beta-1}{\beta+1} \right. \right) - \frac{(1-q)}{(\beta-q)} \sqrt{\beta+1} F \left(\Phi_2 \left| \frac{\beta-1}{\beta+1} \right. \right) \\ &\quad \left. + \sqrt{\beta+1} E \left(\Phi_2 \left| \frac{\beta-1}{\beta+1} \right. \right) \right\} \Big|_{x=1}^q, \end{aligned} \tag{57}$$

where

$$\Phi_2 = \Phi_2(x) = i \sinh^{-1} i \sqrt{\frac{\beta+1}{\beta-x}}. \tag{58}$$

A hint at arriving at the expressions in Eqs. (55) and (57) for the integrals C_1 and C_2 has been provided by Wolfram integrator [45] (see also online supplementary material [46]).

C. Final Result

The exact result for the mean-free path L_d in the diffusive scattering case can be now straightforwardly obtained by substituting Eqs. (55) and (57) into Eq. (52). However, this results in a largely unmanageable expression of limited practical value,

since numerical integration can be performed rather easily. The results obtained by numerical integration are shown in Fig. 3. The Fortran F77 code *jsc2d.f*, which employs the routine *qromo.f* in combination with the routines *polint.f* and *midpnt.f*, all of Numerical Recipes [47], is freely available online [48].

Nevertheless, there is still one important use of the exact analytical results of the preceding sections: they enable one to derive an analytic approximation in the thin-shell limit $D \ll 1$. Bearing on the experience from the spherical shell case [27], one expects that at least the leading term of the asymptotic for $D \ll 1$ can be derived from any of ℓ_1 or ℓ_2 . Indeed, in the thin-shell limit, both ℓ_1 and ℓ_2 should approach the same value. Given that the analytic expression for ℓ_2 [see Eq. (49)] is much simpler than that for ℓ_1 [see Eqs. (52), (55), and (57)], we begin with the former. In the limit $D \rightarrow 0$, one finds, on using the identities in Eqs. (A12)–(A14) in Eq. (49),

$$\begin{aligned} L_{d;\text{asmp}} \sim \ell_2 \sim \frac{2}{\pi} \left\{ r_2 - r_1 + \frac{r_2}{4} (1 - q^2) \ln(1 - q^2) \right. \\ \left. - \frac{r_2}{2} (1 - q^2) \ln(1 - q^2) + r_2 (1 - q^2) \left(\frac{1}{4} - \ln 2 + 2 \ln 2 \right) \right\} \\ \sim \frac{D}{\pi} \ln \left(\frac{R}{2D} + \frac{1}{4} \right) + \frac{2}{\pi} (1 + 2 \ln 2) D + \mathcal{O}(D^2 \ln D). \end{aligned} \quad (59)$$

Interestingly, the leading term asymptotic consisting of the very first term on the right-hand side of Eq. (59) sets in only for (from an experimental point of view) extremely thin shells with $D/R \lesssim 0.1$ (see Fig. 4). In general, both terms in Eq. (59) are required. Surprisingly enough, the two-term asymptotic $L_{d;\text{asmp}}$ given by Eq. (59) describes the exact mean-free path L_d in the diffusive scattering case almost over the entire parameter range of D/R . As illustrated in Fig. 4, $L_{d;\text{asmp}}$ is within 10% of L_d for $D/R \lesssim 0.9$, within $\approx 5\%$ of L_d for $D/R \lesssim 0.5$, within $\approx 2\%$ of L_d for $D/R \lesssim 0.25$, and within 1% of L_d for $D/R \lesssim 0.13$.

5. DISCUSSION

The effect of a *size-corrected* dielectric function [Eq. (3)] for elongated structures is expected to be more pronounced than the effect of the so-called *nonlocal* dielectric function dis-

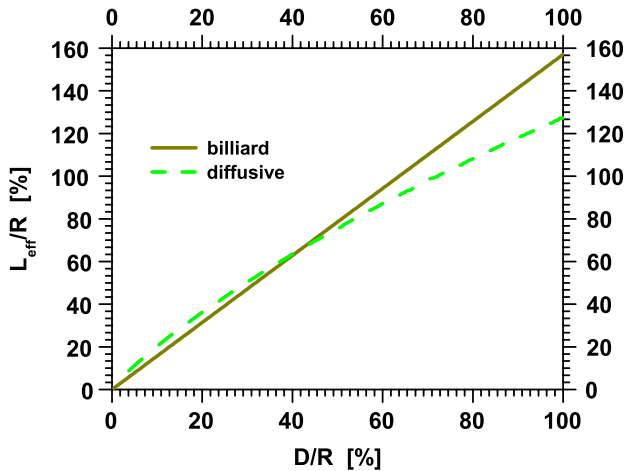


Fig. 3. (Color online) Mean-free path in the cylindrical shell case for the billiard and diffusive scattering models as a function of the ratio D/R , where D is the shell thickness and R is the shell outer radius.

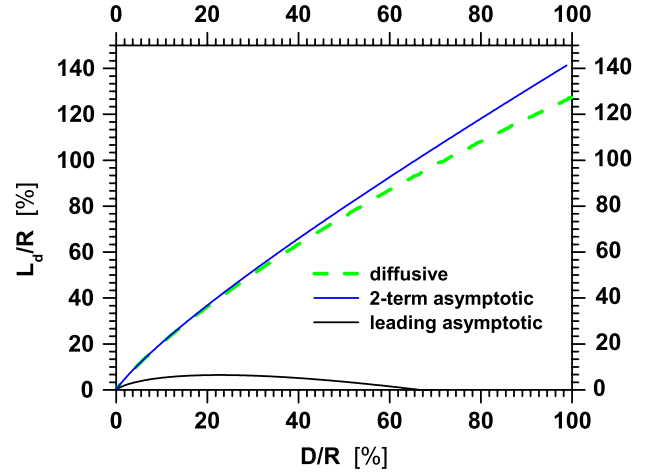


Fig. 4. (Color online) Exact and approximate mean-free path in the cylindrical shell case for the diffusive scattering model as a function of the ratio D/R , where D is the shell thickness and R is the shell outer radius.

cussed by McMahon *et al.* [34]. Indeed, given $v_F = 1.38 \times 10^{15}$ nm/s of gold and $R = 2$ nm in Figs. 1, 2 of [34], one has $L_B = \pi$ nm and $v_F/L_B \approx 724$ THz. The latter value is at least *fortyfold* of the gold bulk damping constant Γ_0 cited in the literature (between ≈ 4.4 and ≈ 18 THz [49]) and roughly 1/3 of the gold plasma frequency ω_p [49].

Since our results are, except for the assumptions regarding the surface scattering, model independent, they apply in principle to any material, or an enclosure, wherein its constituents or components perform a free motion. In the case of nanophotonic and nanoplasmonic applications, the latter presumes free electron metals, such as alkali metals, aluminum, copper, gold, and silver, or suitable semiconductor materials. A threshold length scale below which the free-path effect is expected to be relevant in noble metals is about 15 nm [16,17,50]. (See in this regard the results for nanorods with widths above 15 nm [16] and below 15 nm [17].)

A. Two-Dimensional versus Three-Dimensional Formulas

One can apply $d = 2$ results if and only if the paths along the cylinder, or nanowire, axis are irrelevant for damping. This is expected to be the case if either an external field is applied perpendicularly to the cylinder axis, or an intrinsic optical mode propagating in a nanowire is one of transverse electric (TE) and transverse electromagnetic (TEM) modes, i.e., a mode that does not have any electric field component in the direction of propagation.

The billiard formula in Eq. (28) in the cylindrical shell case cannot be obtained from the general billiard mean-free path L_B given by Eq. (4) for $d = 3$ starting with a circular cylinder of radius r and a finite length ℓ and then taking the limit $\ell \rightarrow \infty$. Indeed, in the latter case,

$$\frac{4|\Omega|}{|\partial\Omega|} = \frac{4\pi r^2 \ell}{2\pi r \ell [1 + (r/\ell)]} \rightarrow 2r. \quad (60)$$

This is because of nonzero contributions of the paths along the cylinder axis. The latter suggests that the billiard formula in Eq. (4) for $d = 3$ has to be used when describing the linewidth of a longitudinal, or long-axis, plasmon (LAP)

of nanorods [16,17,51]. The billiard formula for $d = 2$ may then be relevant for describing the linewidth of a short-axis plasmon (SAP) of nanorods. Unfortunately, a SAP produces a much weaker signature and is thus more difficult to determine experimentally. Consequently, a large body of experimental work only concerns the LAPs [16,17,51].

B. Billiard versus Diffusive Model

In a homogeneous cylinder case, the difference between the billiard and diffusive models of surface scattering is reflected merely by a different slope of the linear dependence of a mean-free path L_{eff} on the cylinder radius R [Eq. (17)]. Similarly to a spherical shell case [27], qualitatively different dependencies on the inner and outer shell radii result for different model cases in the shell geometry (see Fig. 3). A linear behavior of $L_B = \pi D/2$ on the shell thickness D for the billiard model [Eq. (28)] should be contrasted with a complicated functional dependence on the shell thickness D in the diffusive case (see Section 4). Preliminary experimental results in a spherical shell case are compatible with the billiard model and appear to rule out both the Euler diffusive scattering and an isotropic scattering [27]. See in this regard recent experimental results by Lermé *et al.* [50]. Quite amazingly, although Lermé *et al.* [50] did not emphasize it, their experimental data regarding *silver* nanospheres fit nicely to the billiard model [27]. The latter yields for the mean-free path the value of $4R/3$ {e.g., Eq. (141) of [27]}, which, when compared with Eq. (1) of [50], would have yielded $g = 3/4 = 0.75$. The latter value is almost in the middle of an overall experimental value of $g_{\text{exp}} \approx 0.7 \pm 0.1$ determined by Lermé *et al.* [50]. Compared to the billiard model, the diffusive model of Euler and Kreibig would yield, for the mean-free path, the value of R , or $g = 1$ [27]. Therefore, one expects that the billiard model will provide a better description of the free-path effect also for $d = 2$.

C. Radiation Damping and Other Effects

For larger particles the right-hand side of Eq. (1) has to be supplemented with a volume-dependent *radiation damping term* [see Eq. (3) of [16,17]]. Importantly, when determining a size-corrected dielectric function according to Eq. (3), the damping constant in a Drude-like term $\varepsilon_{D,sd}$ in Eq. (3) remains to be $\gamma = \Gamma$, given by the size-corrected value of Eq. (1) *without* the radiative reaction term [24,52]. Indeed, the radiation damping term [52], which can be traced down to the k^3 -dependent *radiative reaction* term in the Abraham–Lorentz equation [see, e.g., Section 16.2 and Eqs. (16.8-9) of [53]], accounts for the linewidth broadening that is *extrinsic* to the dielectric function [24,52].

The free-path effect described in the article could be most easily detected for a dielectric core and metal, or semiconductor, shell. In the case of bimetallic structures, such as those investigated by Liu and Guyot-Sionnest [51], one has to take into account the effect of the so-called *chemical interface damping*: because occupied states in the core and shell region may coincide in their energy, the electronic wave functions of the conduction electrons are transmitted through a metal–metal interface and the electrons are no longer confined by the metal–metal interface.

6. CONCLUSIONS

Mean-free path L_{eff} was calculated for the circular shell geometry that is a special case of the domain that is (i) neither *convex* nor (ii) *simply connected*. For such domains, the early results by Cauchy [35,36] and others [37–42], based on the average projected area of *convex* bodies, could no be longer applied. L_{eff} was calculated under the assumptions of (i) *billiard scattering* and of (ii) *diffusive scattering*. Whereas, for the billiard model, L_{eff} depends linearly on the shell thickness D as $L_{\text{eff}} = \pi D/2$, the mean-free path in the diffusive scattering case is a complicated expression involving complete and incomplete elliptic integrals of the first, second, and third kinds. Nevertheless, a linear combination of D and $D \ln(R/2D)$, where R is the outer circle radius, was shown to capture the functional dependence of L_{eff} in the diffusive scattering case remarkably well over almost the entire parameter range. Similarly to a spherical shell geometry, circular shell geometry enables us to distinguish between the different models of electron scattering. Hopefully, this would be performed in future experiments on single and well-controlled dielectric-core–metal-shell nanowires.

APPENDIX A: SUMMARY OF ELEMENTARY FORMULAS

$$\int_a^b \cos^2 \theta d\theta = \frac{b-a}{2} + \frac{1}{4}(\sin 2b - \sin 2a), \quad (\text{A1})$$

$$\int \sqrt{a^2 - x^2} dx = \frac{x}{2} \sqrt{a^2 - x^2} + \frac{a^2}{2} \arcsin \frac{x}{|a|}, \quad (\text{A2})$$

$$\begin{aligned} \int \frac{\sqrt{1-x^2}}{x-\beta} dx &= - \int \frac{x+\beta}{\sqrt{1-x^2}} dx - (\beta^2 - 1) \int \frac{1}{(x-\beta)\sqrt{1-x^2}} dx \\ &= \sqrt{1-x^2} - \beta \arcsin x \\ &\quad + \sqrt{\beta^2 - 1} \arcsin \frac{1-\beta x}{x-\beta}, \end{aligned} \quad (\text{A3})$$

$$\int \frac{1}{(x-\beta)\sqrt{1-x^2}} dx = - \frac{1}{\sqrt{\beta^2 - 1}} \arcsin \frac{1-\beta x}{x-\beta}, \quad (\text{A4})$$

$$\int \frac{dx}{\sqrt{1-x^2}} = \arcsin x, \quad (\text{A5})$$

$$\int \frac{x dx}{\sqrt{1-x^2}} = -\sqrt{1-x^2}, \quad (\text{A6})$$

$$\frac{1-\beta x}{x-\beta} = \begin{cases} 1, & x = 1 \\ -q, & x = q \end{cases}. \quad (\text{A7})$$

All the integration formulas can be straightforwardly verified by a direct differentiation. Equation (A2) can be independently found as formula (1.2.46.8) of [43]. The first equality in Eq. (A3) follows by a straightforward recasting of the

integrand. The final result in Eq. (A3) can also be verified by combining Eqs. (A4)–(A6). Equation (A4) is given as Eq. (1.2.53.15) of [43], whereas Eqs. (A5) and (A6) are elementary integrals.

The incomplete elliptic integrals F , E , and Π of the first, second, and third kind, respectively, are defined by

$$F(\phi, m) = \int_0^\phi \frac{d\theta}{\sqrt{1 - m \sin^2 \theta}}, \quad (\text{A8})$$

$$E(\phi, m) = \int_0^\phi \sqrt{1 - m \sin^2 \theta} d\theta, \quad (\text{A9})$$

$$\Pi(n, \phi, n) = \int_0^\phi \frac{d\theta}{(1 - n \sin^2 \theta) \sqrt{1 - m \sin^2 \theta}}. \quad (\text{A10})$$

The above integrals are, in principle, defined for any value of m and n . One often speaks about elliptic integrals only if the range of m and n parameters is limited to $0 \leq m, n \leq 1$ [43,44]. One has [see Eqs. (17.3.26), (17.3.27) of [44]]

$$K(q^2) - E(q^2) \sim \frac{\pi}{4} q^2 \quad (q \rightarrow 0), \quad (\text{A11})$$

$$K(q^2) \sim \frac{1}{2} \ln \frac{16}{1 - q^2} = -\frac{1}{2} \ln(1 - q^2) + 2 \ln 2 \quad (q \rightarrow 1_-), \quad (\text{A12})$$

$$E(q^2) \sim 1 - \frac{(1 - q^2)}{4} \ln(1 - q^2) - (1 - q^2) \left(\frac{1}{4} - \ln 2 \right) \quad (q \rightarrow 1_-). \quad (\text{A13})$$

Regarding the thin-shell limit $D = r_2 - r_1 \rightarrow 0$, the following expressions have been repeatedly used:

$$1 - q^2 = 1 - \frac{(R - D)^2}{R^2} = \frac{2D}{R} - \frac{D^2}{R^2} = \frac{2D}{R} \left(1 - \frac{D}{2R} \right), \quad (\text{A14})$$

$$\frac{1}{1 - q^2} \sim \frac{R}{2D} \left(1 + \frac{D}{2R} \right) = \frac{R}{2D} + \frac{1}{4}. \quad (\text{A15})$$

ACKNOWLEDGMENTS

I thank Professor C. F. Bohren for discussion and for calling my attention to the early work by Cauchy and Dirac.

REFERENCES AND NOTES

- B. Dubertret, M. Calame, and A. J. Libchaber, "Single-mismatch detection using gold-quenched fluorescent oligonucleotides," *Nat. Biotechnol.* **19**, 365–370 (2001).
- J. R. Lakowicz, "Radiative decay engineering: biophysical and biomedical applications," *Anal. Biochem.* **298**, 1–24 (2001).
- A. Moroz, "A recursive transfer-matrix solution for a dipole radiating inside and outside a stratified sphere," *Ann. Phys.* **315**, 352–418 (2005).
- A. Moroz, "Spectroscopic properties of a two-level atom interacting with a complex spherical nanoshell," *Chem. Phys.* **317**, 1–15 (2005).
- A. Moroz, "Non-radiative decay of a dipole emitter close to a metallic nanoparticle: importance of higher-order multipole contributions," *Opt. Commun.* **283**, 2277–2287 (2010).
- S. Pillai, K. R. Catchpole, T. Trupke, and M. A. Green, "Surface plasmon enhanced silicon solar cells," *J. Appl. Phys.* **101**, 093105 (2007).
- G. Raschke, S. Kowarik, T. Franzl, C. Sönnichsen, T. A. Klar, J. Feldmann, A. Nichtl, and K. Kürzinger, "Biomolecular recognition based on single gold nanoparticle light scattering," *Nano Lett.* **3**, 935–938 (2003).
- A. D. McFarland and R. P. Van Duyne, "Single silver nanoparticles as real-time optical sensors with zeptomole sensitivity," *Nano Lett.* **3**, 1057–1062 (2003).
- G. Raschke, S. Brogl, A. S. Susha, A. L. Rogach, T. A. Klar, J. Feldmann, B. Fieres, N. Petkov, T. Bein, A. Nichtl, and K. Kürzinger, "Gold nanoshells improve single nanoparticle molecular sensors," *Nano Lett.* **4**, 1853–1857 (2004).
- L. J. Sherry, S.-H. Chang, G. C. Schatz, R. P. Van Duyne, B. J. Wiley, and Y. Xia, "Localized surface plasmon resonance spectroscopy of single silver nanocubes," *Nano Lett.* **5**, 2034–2038 (2005).
- L. J. Sherry, R. Jin, C. A. Mirkin, G. C. Schatz, and R. P. Van Duyne, "Localized surface plasmon resonance spectroscopy of single silver triangular nanoprisms," *Nano Lett.* **6**, 2060–2065 (2006).
- F. Hao, Y. Sonnefraud, P. Van Dorpe, S. A. Maier, N. J. Halas, and P. Nordlander, "Symmetry breaking in plasmonic nanocavities: subradiant LSPR sensing and a tunable Fano resonance," *Nano Lett.* **8**, 3983–3988 (2008).
- N. Verellen, Y. Sonnefraud, H. Sobhani, F. Hao, V. V. Moshchalkov, P. Van Dorpe, P. Nordlander, and S. A. Maier, "Fano resonances in individual coherent plasmonic nanocavities," *Nano Lett.* **9**, 1663–1667 (2009).
- W. H. Yang, G. C. Schatz, and R. P. Van Duyne, "Discrete dipole approximation for calculating extinction and Raman intensities for small particles with arbitrary shapes," *J. Chem. Phys.* **103**, 869–875 (1995).
- J. B. Jackson, S. L. Westcott, L. R. Hirsch, J. L. West, and N. J. Halas, "Controlling the surface enhanced Raman effect via the nanoshell geometry," *Appl. Phys. Lett.* **82**, 257–259 (2003).
- C. Sönnichsen, T. Franzl, T. Wilk, G. von Plessen, J. Feldmann, O. Wilson, and P. Mulvaney, "Drastic reduction of plasmon damping in gold nanorods," *Phys. Rev. Lett.* **88**, 077402 (2002).
- C. Novo, D. Gomez, J. Perez-Juste, Z. Zhang, H. Petrova, M. Reisman, P. Mulvaney, and G. V. Hartland, "Contributions from radiation damping and surface scattering to the linewidth of the longitudinal plasmon band of gold nanorods: a single particle study," *Phys. Chem. Chem. Phys.* **8**, 3540–3546 (2006).
- U. Kreibig, "Electronic properties of small silver particles: the optical constants and their temperature dependence," *J. Phys.* **F 4**, 999–1014 (1974).
- U. Kreibig and C. V. Fragstein, "The limitation of electron mean free path in small silver particles," *Z. Phys. A* **224**, 307–323 (1969).
- F. W. Reynolds and G. R. Stilwell, "Mean free paths of electrons in evaporated metal films," *Phys. Rev.* **88**, 418–419 (1952).
- J. Euler, "Infrared properties of metals and the mean free paths of conduction electrons," *Z. Phys.* **137**, 318–332 (1954).
- U. Kreibig and L. Genzel, "Optical absorption of small metallic particles," *Surf. Sci.* **156**, 678–700 (1985).
- C. F. Bohren and D. R. Huffman, *Absorption and Scattering of Light by Small Particles* (Wiley, 1998).
- A. Moroz, "Depolarization field of spheroidal particles," *J. Opt. Soc. Am. B* **26**, 517–527 (2009).
- N. Chernov, "Entropy, Lyapunov exponents and mean free path for billiards," *J. Stat. Phys.* **88**, 1–29 (1997).
- N. Chernov and R. Markarian, *Introduction to the Ergodic Theory of Chaotic Billiards*, online book available at <http://www.math.uab.edu/chemov/papers/rbook.pdf>.
- A. Moroz, "Electron mean-free path in a spherical shell geometry," *J. Phys. Chem. C* **112**, 10641–10652 (2008).
- H. van der Lem and A. Moroz, "Towards two-dimensional complete photonic band gap structures below infrared wavelengths," *J. Opt. A Pure Appl. Opt.* **2**, 395–399 (2000).

29. R. M. Dickson and L. A. Lyon, "Unidirectional plasmon propagation in metallic nanowires," *J. Phys. Chem. B* **104**, 6095–6098 (2000).
30. Z.-X. Zhang, M.-L. Hu, K. T. Chan, and C.-Y. Wang, "Plasmonic waveguiding in a hexagonally ordered metal wire array," *Opt. Lett.* **35**, 3901–3903 (2010).
31. J. Takahara, S. Yamagishi, H. Taki, A. Morimoto, and T. Kobayashi, "Guiding of a one-dimensional optical beam with nanometer diameter," *Opt. Lett.* **22**, 475–478 (1997).
32. Y. Zhang and H. Dai, "Formation of metal nanowires on suspended single-walled carbon nanotubes," *Appl. Phys. Lett.* **77**, 3015–3017 (2000).
33. V. Poborchii, T. Tada, T. Kanayama, and A. Moroz, "Silver-coated silicon-pillar photonic crystals: enhancement of a photonic band gap," *Appl. Phys. Lett.* **82**, 508–510 (2003).
34. J. M. McMahon, S. K. Gray, and G. C. Schatz, "Nonlocal optical response of metal nanostructures with arbitrary shape," *Phys. Rev. Lett.* **103**, 097403 (2009).
35. A. Cauchy, "Memoire sur la rectification des courbes et la quadrature des surfaces courbes," (Paris, 1832). Reprinted in *Oeuvres Complètes*, 1st series, (Gauthiers Villars, 1908), Vol. 2, p. 167. A short account of these results in the form of theorems was later published in [36], but no formal proof was given.
36. A. Cauchy, "Note sur divers théorèmes relatifs à la rectification des courbes et à la quadrature des surfaces," *C. R. Acad. Sci.* **13**, 1060–1063 (1841).
37. E. Czuber, "Zur Theorie der geometrischen Wahrscheinlichkeiten," *Sitzungsberichte der mathematisch-naturwissenschaftliche Klasse der Kaiserlichen Akademie der Wissenschaften Wien* **90**, 719–742 (1884).
38. P. A. M. Dirac, "Approximate rate of neutron multiplication for a solid of arbitrary shape and uniform density," *British Report MS-D-5, Part I* (1943).
39. A. M. Weinberg and E. P. Wigner, *The Physical Theory of Neutron Chain Reactors* (Univ. of Chicago Press, 1958).
40. V. Vouk, "Projected area of convex bodies," *Nature* **162**, 330–331 (1948).
41. W. J. M. de Kruijf and J. L. Kloosterman, "On the average chord length in reactor physics," *Ann. Nucl. Energy* **30**, 549–553 (2003).
42. E. A. Coronado and G. C. Schatz, "Surface plasmon broadening for arbitrary shape nanoparticles: a geometrical probability approach," *J. Chem. Phys.* **119**, 3926–3934 (2003).
43. A. P. Prudnikov, Yu. A. Brychkov, and O. I. Marichev, *Integrals and Series*, 2nd ed. (Gordon and Breach, 1988).
44. M. Abramowitz and I. A. Stegun, *Handbook of Mathematical Functions* (Dover, 1973).
45. Wolfram Mathematica online integrator available at <http://integrals.wolfram.com>.
46. Online supplementary material is available at <http://www.wave-scattering.com/fsc2D-suppl.pdf>.
47. W. H. Press, S. A. Teukolsky, W. T. Vetterling, and B. P. Flannery, *Numerical Recipes in Fortran 77* (Cambridge Univ. Press, 2001) (see also <http://www.nr.com>).
48. The Fortran F77 code is freely available at <http://www.wave-scattering.com/fsc2d.f>.
49. See a compilation of Drude fit parameters of various metals at <http://www.wave-scattering.com/drudedefit.html>.
50. J. Lermé, H. Baida, C. Bonnet, M. Broyer, E. Cottancin, A. Crut, P. Maioli, N. Del Fatti, F. Valle, and M. Pellarin, "Size dependence of the surface plasmon resonance damping in metal nanospheres," *J. Phys. Chem. Lett.* **1**, 2922–2928 (2010).
51. M. Liu and P. Guyot-Sionnest, "Synthesis and optical characterization of Au/Ag core/shell nanorods," *J. Phys. Chem. B* **108**, 5882–5888 (2004). There is apparently no physical reason for the denominator in their formula (6).
52. A. Wokaun, J. P. Gordon, and P. F. Liao, "Radiation damping in surface-enhanced Raman scattering," *Phys. Rev. Lett.* **48**, 957–960 (1982).
53. J. D. Jackson, *Classical Electrodynamics*, 3rd ed. (Wiley, 1999).